

ALTERNATIVE LIDAR TECHNOLOGIES FOR STOCKPILE MONITORING AND REPORTING

Y. Koshan¹, R. Manish¹, M. Joseph¹, A. Habib¹ *

¹ Lyles School of Civil Engineering, Purdue University, West Lafayette, IN 47907, USA – (ykoshan, rmanish, mjosephf, ahabib)@purdue.edu

KEY WORDS: Stockpile, Volume Estimation, LiDAR, Registration, System Calibration.

ABSTRACT:

Accurate volume estimation of salt stockpiles stored in covered facilities is essential for effective management and budgeting in the transportation industry. Due to environmental concerns, salt is stored in indoor facilities. The surveying tools that are widely applied for outdoor stockpile estimation such as Global Navigation Satellite System (GNSS) Receivers and Uncrewed Aerial Vehicles (UAV) are not applicable for indoor mapping. To address this limitation, our prior research proposed and developed a Stockpile Monitoring and Reporting Technology (SMART) which was designed for indoor stockpile volume estimation. This study builds upon that prior research to evaluate the feasibility and performance of different LiDAR alternatives within the SMART system. Three LiDAR sensors (Velodyne VLP-16, Ouster OS1-32-U, and Blickfeld Cube 1) are compared in terms of system calibration, point cloud registration, and volume estimation. Results demonstrate the impact of LiDAR sensor choice on system performance, occlusion rates, and volumetric accuracy. The findings contribute to expanding the versatility and adaptability of LiDAR technology in SMART applications, allowing for more efficient and accurate stockpile volume estimation.

1. INTRODUCTION

Stockpile volume estimation is crucial for a variety of fields, including construction, agriculture, and mining. In transportation, salt material is used for road de-icing during the winter season (Decai et al., 2021). Due to environmental concerns, salt is stored in covered facilities (Kelly, 2018), which complicates accurate and effective volume estimation of the material using conventional surveying techniques, such as RTK survey (He et al., 2019) and UAV data collection (Yilmaz, 2010).

Each year, the Indiana Department of Transportation (INDOT) spends between \$30 to \$60 million on the purchase and transport of salt across the state (Mahlberg et al., 2022). To effectively manage their budget, it is crucial to continuously and accurately monitor the amount of salt in the inventory. Conventional techniques of volume assessment using haul tickets, loader counting, and visual inspection are inefficient (Raeva et al., 2016).

To address these limitations, our prior research proposed an indoor stockpile volume estimation technology that used a multi-sensor platform known as *Stockpile Monitoring and Reporting Technology* (SMART) that is comprised of two LiDAR sensors and one RGB camera (Manish et al. 2022). SMART has been developed into several mapping platforms and field-tested at more than hundred salt storage facilities in Indiana, USA (Mahlberg et al., 2022).

This study goes further into investigating various LiDAR alternatives for the SMART system to address some of the emerging challenges associated with the scalability and portability of the platform. To be specific, three LiDAR alternatives – Velodyne VLP16, Ouster OS1-32-U, and Blickfeld Cube 1 Outdoor, each with various advantageous features are utilized in this study to assess their performance in stockpile monitoring.

2. PROBLEM STATEMENT AND RESEARCH OBJECTIVES

Considering the rapid advancements in LiDAR technology and the growing demand, it is crucial to expand the scope of LiDAR usage in SMART applications and make it adaptable to emerging sensors. For instance, the Ouster OS1-32-U is a spinning multi-beam LiDAR sensor that offers a higher point cloud density and vertical field of view compared to the VLP16. Another example is the Blickfeld Cube 1, a solid-state LiDAR that eliminates rotating elements, making it more durable in harsh environments and extending its lifespan. As of now, the impact of employing the above LiDAR sensors on the performance of various SMART data acquisition and post-processing procedures needs investigation.

This study aims to evaluate different LiDAR alternatives in the SMART system considering their feasibility and performance for the following main operations:

- System calibration,
- Point cloud registration, and
- Volume estimation

3. SYSTEM AND DATASET DESCRIPTION

3.1 System Description and Data Collection Strategies

As shown in Figure 1, the main components of a Velodyne-based SMART system are an RGB camera (GoPro Hero 9), two Velodyne VLP16 LiDAR sensors, a circuit case, and a tripod to support the sensor assembly (Manish et al., 2022). For the Ouster variant of the SMART system, the Velodyne units are substituted with two Ouster OS-1-32-U LiDAR sensors, as shown in Figure 2(a). Using two LiDAR units facilitates covering a larger area while maintaining high-point cloud density. The RGB camera on these two platforms serves as a tool for the coarse alignment of the acquired LiDAR data (Hasheminasab et al., 2023). It also provides a visual record of the stockpile in the storage facility.

* Corresponding author

The circuit case includes a Raspberry Pi 4 computer which is used to trigger the LiDAR sensors and store their measurement data. One should note that all these components on the Velodyne or Ouster SMART are powered by a single source, a lithium-polymer battery. The third SMART variant consists of two Blickfeld Cube 1 Outdoor LiDAR units (as shown in Figure 2(b)) that are powered using power over Ethernet (PoE) devices. A graphical user interface (GUI), provided by the manufacturer, is used to control, capture, and store LiDAR scans on an external computer. The Blickfeld SMART system doesn't include an RGB camera. A brief summary of each SMART variant is described below, and all the technical characteristics of the three LiDAR sensors and GoPro camera are listed in Tables 1 and 2, respectively (Blickfeld Cube 1, 2023; Ouster OS1 Sensor, 2023; Velodyne VLP16 Puck, 2023; GoPro Hero 9 Black, 2023)

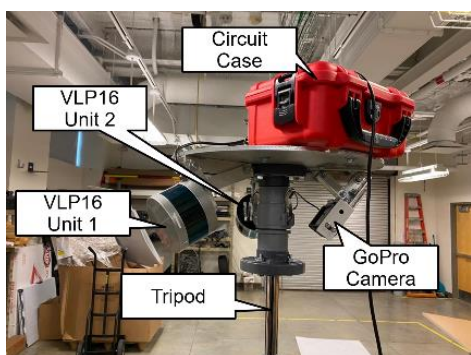


Figure 1. SMART (Velodyne) system components.

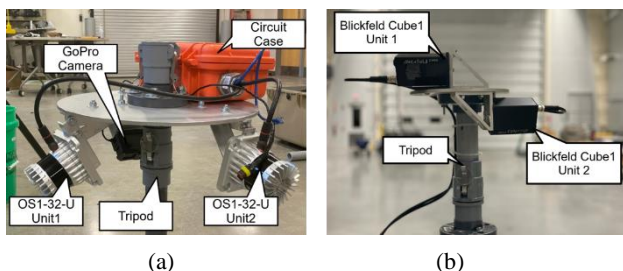


Figure 2. Variants of the SMART system: (a) Ouster LiDAR and (b) Blickfeld LiDAR.

	LiDAR Sensor		
	Velodyne VLP-16 (Puck)	Ouster OS1-32-U	Blickfeld Cube 1 (Outdoor)
Field of View (H×V)	360°×30°	360°×45°	70°×30°
Maximum Range	100 m	100 m	75 m
Range Accuracy	3 cm	3 cm	<2 cm
Scanning Rate (Single return)	300,000 points/sec (10 Hz)	655,360 points/sec (10 Hz)	48,165 Points/sec (9.5 Hz)
Sensor Weight	830 g	447 g	330 g
Ingress Protection Rating (IP)	67	69K	65

Table 1. Technical characteristics of utilized LiDAR sensors.

	Camera
Camera Model	GoPro Hero 9
Camera Type	RGB Frame Camera
Focal Length	3 mm
Image Dimensions	5184 x 3888 pixels
Pixel Size	4.5 μm
Operating Temperature	-10°C to 35°C
Wavelength Range	400-700 nm
Spectral Bands	3 Bands

Table 2. Technical characteristics of the RGB camera used in the Velodyne and Ouster SMART units.

3.1.1 Velodyne SMART: As mentioned in Table 1, point clouds derived from the VLP-16 LiDAR have a range accuracy of 3 cm with a maximum reach of 100 m. This LiDAR is capable of two preset scan rates of 10 and 20 Hz. At the default rate of 10 Hz and single return mode, the VLP16 captures 300,000 points per second. In general, the environment inside salt storage facilities is harsh for electronics and sensitive instruments. In that regard, it is worth mentioning that most LiDAR sensors these days have a certain level of environmental protection, indicated by Ingress Protection (IP) rating, should they be used under harsh conditions (IP ratings, 2023). The VLP-16 LiDAR is rated IP67, according to which, it is protected against dust (xx6x) and the effects of temporary immersion in water (xxx7).

The Velodyne SMART unit is operated on an extendable tripod at a height of 19 ft and horizontally rotated by 360°. Rotations are performed in 30° increments, wherein LiDAR sensors scan four sides, each with 30° coverage. Such sensor configuration allows for successful LiDAR data registration even with small overlap between successive scans. The coverage of the Velodyne SMART in each scan is illustrated in Figure 3, where blue and cyan colored point clouds represent the LiDAR coverage at a given rotation increment, while the gray colored points represent the facility's point cloud (filtered by height in the range of 0-4 m) captured by all scans. Concurrently, the camera captures images with a 118° horizontal coverage. To improve the overall coverage and reduce occlusions in LiDAR scans, multiple stations may be used during the data collection. Here, the number of stations depends on the facility size and stockpile configuration in the facility.

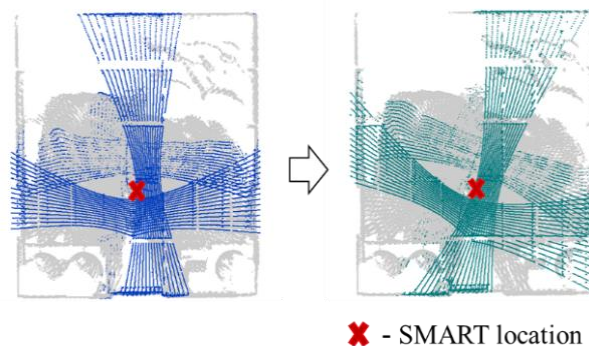


Figure 3. LiDAR coverage (SMART Velodyne) of a facility in successive rotations.

3.1.2 Ouster SMART: Although there are some similarities between Velodyne and Ouster sensors from the operational perspective, the Ouster unit used in this study (OS-1-32-U) shows distinctive advantages over VLP-16. Unlike the Velodyne unit, this sensor has a FoV of $360^{\circ} \times 45^{\circ}$. Ouster-derived distances are accurate to within 3 cm at a maximum range of 100 m, which is the same as VLP16's. However, for an identical scan rate of 10 Hz, Ouster-derived point clouds are denser with 655,360 points captured per second, all attributed to the Ouster's 32-beam LiDAR (compared to 16 for VLP-16). Furthermore, Ouster has the highest IP rating compared to the other two sensors used in this study. The IP69K rating provides protection against dust and high-pressure water jets at high temperatures.

Data collection strategy for the Ouster SMART is identical to the procedure followed for the Velodyne SMART. Accordingly, the wider coverage of Ouster compared to Velodyne (45° vs. 30°) therefore results in a point cloud with overall higher density. The increased coverage also enables capturing a relatively larger area and scanning of more common features between consecutive scans for the same rotational increments.

3.1.3 Blickfeld SMART: In contrast to the Velodyne and Ouster sensors utilized in this study, the Blickfeld Cube 1 sensor has a narrower field of view (FoV) of $70^{\circ} \times 30^{\circ}$. This limitation was partially solved by mounting the two units in such a way that combined the shorter FoV for a collectively larger vertical coverage. Among the advantages of Cube 1 over the other two LiDAR units, its derived distances are accurate to within 2 cm at a maximum range of 75 m. Moreover, Cube 1 can be configured to capture data in the form of 30 to 400 scanlines at a variable rate of up to 50 Hz. The selected scan rate for this study is 9.5 Hz that captures 48,165 points per second in 30 scan lines. Compared to the Velodyne and Ouster unit, this sensor has a lower IP rating of IP65. Yet, that rating still ensures reasonable protection against dust and low-pressure water jets.

During data acquisitions, Blickfeld SMART utilizes an extendable tripod with the average height of 16 ft. Compared to other SMART units that capture LiDAR data in four directions simultaneously, Blickfeld SMART can scan only one direction at a time (even considering the combined FoV of two sensors). The narrow, window-shaped field of view of the Blickfeld SMART imposes certain limitations. In some locations, the maximum height at which the unit can be raised is restricted, as it may result in the occlusion of ground or lower areas of the stockpile. Moreover, due to the smaller FoV of LiDAR, features used in point cloud registration are limited only to those in overlapping regions among consecutive scans. For this reason, the rotation increments are kept smaller, in the range of 5° to 10° .

For better visualization, Figure 4 illustrates the Blickfeld LiDAR coverage during a 10° horizontal rotation. The green and yellow point clouds represent the LiDAR coverage before and after the rotation, respectively. The gray colored points in Figure 4 indicate the ground surface of the facility, similar to those in Figure 3. From Figure 4, it can be seen that the two point clouds have limited coverage (unlike the 4-sided coverage of Velodyne and Ouster). As in the case of the other two systems, Blickfeld SMART can be employed at multiple stations to capture more salt surface and reduce occlusion, with the number of stations determined by the facility size and stockpile configuration in the facility.

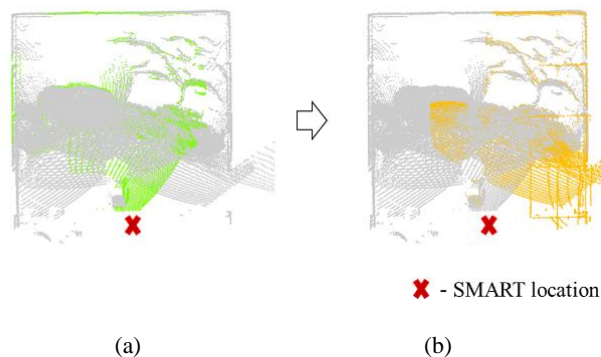


Figure 4. Coverage of individual LiDAR scans from Blickfeld SMART, capturing (a) the central and (b) right sides of a facility.

3.1.4 Hovermap ST: In addition to the three SMART variants, a fourth system, Emesent Hovermap ST, which is a simultaneous localization and mapping (SLAM)-based mobile 3D scanning system (Figure 5), was used as a reference for the experimental results. This system employs a rotating 16-beam LiDAR to cover surrounding areas and provides a FoV of $360^{\circ} \times 290^{\circ}$ (HOVERMAP, 2023).



Figure 5. Emesent Hovermap ST.

Mapping of a salt facility with Hovermap is accomplished by carrying the system over and around the stockpile, as shown in Figure 6. This way, Hovermap is able to acquire a more complete scan of the surface with minimum occlusion. On the downside, this data acquisition procedure poses a major safety hazard for the operator, unlike any of the SMART systems.



Figure 6. Mapping a salt storage facility with Hovermap.

3.2 Datasets Description

The study focuses on two main data collection sites located in West Lafayette, Indiana: 1) Indiana Corn and Soybean Innovation Center (ICSIC), which was used to conduct system calibration for all SMART units, and 2) US 231 salt facility, which was utilized to evaluate the performance and accuracy of the systems. Information regarding the number of stations and number of scans per station for all SMART units at each data collection site is summarized in Table 3.

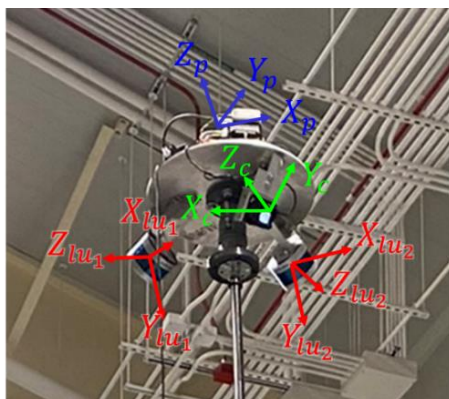
Facility	SMART Velodyne		SMART Ouster		SMART Blackfeld	
	# of Stations	# of Scans Per Station	# of Stations	# of Scans Per Station	# of Stations	# of Scans Per Station
ICSIC	4	13	4	13	5	2
US 231	3	13	2	12	3	3

Table 3. Summary of data collection parameters (number of stations and scans per station) for all SMART units.

4. METHODOLOGY

4.1 System Calibration

SMART system calibration aims at determining the interior orientation parameters (IOP) of the camera (for Velodyne and Ouster SMART), IOP of the two LiDAR units (for all three SMART systems), and individual sensor's mounting parameters with respect to platform body. IOP estimation for the camera involves the evaluation of principal point coordinates, focal length, and distortion parameters. For a LiDAR unit, its IOP includes parameters for defining range measurement and orientation of laser beams relative to the laser unit reference frame. Figure 7 illustrates the coordinate systems for various sensors mounted on a Velodyne SMART. Here, mounting parameters define the offset and orientation of these sensors with respect to the pole coordinate system.



$X_p Y_p Z_p$: Pole coordinate system
 $X_{lu_j} Y_{lu_j} Z_{lu_j}$: j^{th} LiDAR unit coordinate system
 $X_c Y_c Z_c$: Camera coordinate system

Figure 7. Definition of coordinate systems for various sensors on SMART Velodyne/Ouster.

In this study, the LiDAR units' IOP were provided by the manufacturer. For camera IOP, an indoor calibration procedure

was implemented (Manish et al., 2022). The calibration involves using a test field containing multiple checkerboard targets, where ground distances between the targets are known. The image coordinates of the targets are manually measured. As the final step, a bundle adjustment with self-calibration is performed. System calibration of the SMART system to obtain mounting parameters is based on mathematical models for image and LiDAR-based 3D reconstructions, as given by Equations 1 and 2 respectively (Manish et al., 2022).

$$\mathbf{r}_i^m = \mathbf{r}_{p(k)}^m + \mathbf{R}_{p(k)}^m \mathbf{r}_c^p + \lambda(i, c, k) \mathbf{R}_{p(k)}^m \mathbf{R}_c^p \mathbf{r}_i^{c(k)} \quad (1)$$

$$\mathbf{r}_I^m = \mathbf{r}_{p(k)}^m + \mathbf{R}_{p(k)}^m \mathbf{r}_{lu_j}^p + \mathbf{R}_{p(k)}^m \mathbf{R}_{lu_j}^p \mathbf{r}_I^{lu_j(k)} \quad (2)$$

In Equation 1, $\mathbf{r}_i^{c(k)}$ is the vector from the camera perspective center $c(k)$ to an image point i in the camera frame captured at scan k ; $\lambda(i, c, k)$ is the scale factor for the image point i captured by camera c at scan k ; $\mathbf{r}_{p(k)}^m$ and $\mathbf{R}_{p(k)}^m$ are, respectively, position parameters and orientation matrix of the pole frame coordinate system relative to the mapping frame at scan k ; and \mathbf{r}_c^p and \mathbf{R}_c^p are, respectively, lever arm parameters and boresight matrix for the camera relative to pole frame. In Equation 2, $\mathbf{r}_I^{lu_j(k)}$ is the position of an object point I with respect to the j^{th} LiDAR unit frame captured at scan k ; $\mathbf{r}_{lu_j}^p$ and $\mathbf{R}_{lu_j}^p$ are, respectively, lever arm parameters and boresight matrix for LiDAR unit j relative to the pole frame.

During the calibration procedure, planar features from LiDAR scans and point features from images are manually extracted. The mounting parameters are then estimated through an optimization process that minimizes discrepancies among corresponding object features from different LiDAR scans and overlapping images (Ravi et al., 2018), as illustrated in Figure 8.

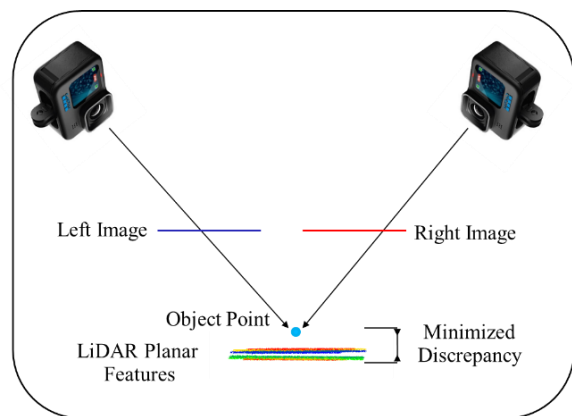


Figure 8. Calibration procedure of minimizing discrepancies among camera and LiDAR features.

4.1.1 Velodyne and Ouster Calibration Strategy: For these systems, the tripod was placed at four stations in a diamond-shaped pattern, as illustrated in Figure 9. These locations provided the LiDAR units a sufficient coverage of features within the facility. During data acquisition at each station, the system is rotated 360 degrees about the Z axis of the pole coordinate system with 30-degree increments. At each increment, LiDAR and imagery data are captured.

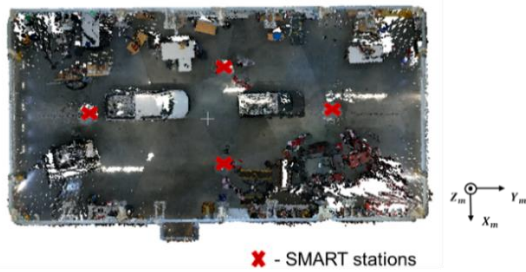


Figure 9. Calibration stations for Velodyne and Ouster SMART units (visualized over Velodyne SMART point cloud).

4.1.1 Blickfeld Calibration Strategy: As discussed earlier, the limited FoV of the Blickfeld SMART requires a different point cloud registration (and therefore calibration) procedure. Although the calibration was conducted in the same facility, instead of capturing the entire region, the area of interest (AoI) was limited to the North-West edge/corner of the building. The AoI was scanned from 5 stations with 2 scans captured at each station. Figure 10 illustrates the AoI and the 5 stations inside the facility. The horizontal rotation between consecutive scans did not exceed 10°. Figure 11 shows the AoI covered from each station and the combined point cloud, where each station captured mostly the northern section of the ICSIC building.

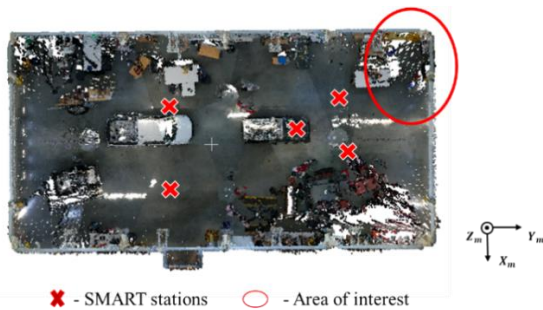


Figure 10. Area of interest and calibration stations for the Blickfeld SMART (visualized over Velodyne SMART point cloud).



Figure 11. LiDAR data from individual and all (combined) stations acquired from Blickfeld SMART (top view).

Given that the Blickfeld SMART scans only one direction of the surrounding environment (unlike the Velodyne and Ouster SMART), system calibration for the Blickfeld unit required overlapping planar features from different scans/stations. Despite that, Blickfeld's point clouds had limited coverage and less-than-ideal feature distribution for the calibration. As a result of this calibration approach, one can expect relatively larger misalignments among common features located very far in the scans, compared to those in the Velodyne and Ouster SMART.

4.2 Post-processing and Volume Estimation

Velodyne and Ouster SMART units employ the procedure described by Manish et al. (2022). GoPro images are used for coarse registration of individual LiDAR scans, while fine registration is conducted using LiDAR features (planar and linear). The quality of LiDAR point cloud alignment after coarse and fine registration steps can be observed from the example in Figure 12. The whole procedure is executed automatically.

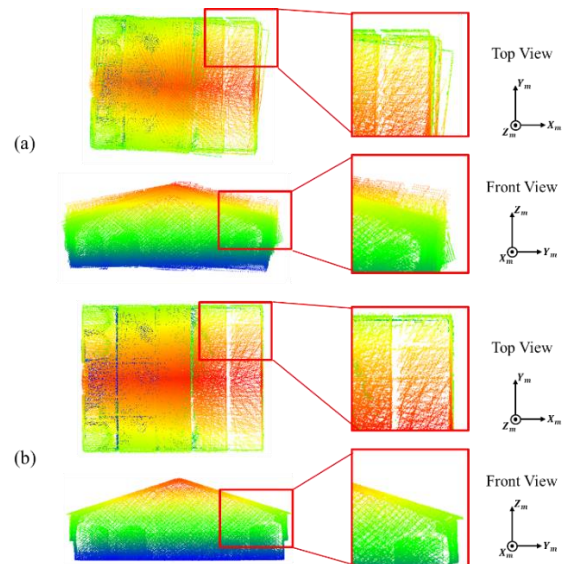


Figure 12. Point clouds of a facility after conducting (a) coarse and (b) fine registration (from the Velodyne SMART).

In the final step, the fine-registered point clouds are further used to estimate the volume of stockpile in the facility. Depending on the geometry of the stored salt, part of the stockpile can be occluded in the LiDAR point cloud. To resolve this issue, occluded areas are interpolated using the facility walls as boundaries, as demonstrated in Figure 13.

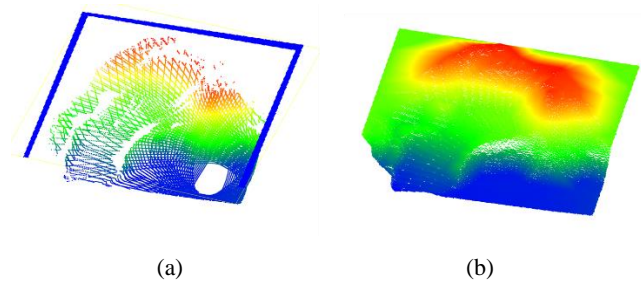


Figure 13. Point clouds of the stockpile area, (a) original surface, and (b) interpolated surface (blue outline represents facility boundary).

5. RESULTS AND DISCUSSION

5.1 Experimental Results

The salt storage facility US 231 was scanned using all SMART units (Velodyne, Ouster, and Blickfeld) as well as Hovermap ST. Volume estimation results are summarized in Table 4. Hovermap was able to capture the stockpile without any occlusion, while the occlusion rate of SMART units ranged from 42.38% to 49.64%. Among the different SMART systems, the Ouster unit delivered a point cloud with the smallest occlusion percentage, mainly due to the highest vertical FoV of the sensor compared to the other two SMART units. The Blickfeld unit, despite having the highest occlusion rate, achieved similar level of volumetric accuracy compared to other units.

#	Scanning System	Estimated Volume (m ³)	Occlusion (%)	Error (%)
1	Hovermap ST	949	0	Reference
2	SMART Blickfeld	1,006	49.64	6.00
3	SMART Ouster	997	42.38	5.06
4	SMART Velodyne	1,007	46.81	6.22

Table 4. Volume estimation results for Hovermap ST and SMART units (US 231 salt facility).

5.2 Discussion

The lower volumetric accuracy observed among all SMART units in comparison to the results presented by Manish et al. (2022), can be attributed to the configuration of the stockpile in the facility. For the dataset used in this study, most of the salt was stored in a cone-shaped pile situated on the left side of the facility, as visualized in Figure 14. This particular configuration poses a challenge for the SMART units as they are unable to capture areas of the stockpile that cannot be accurately interpolated. Figure 15 shows point clouds of the stockpile area derived from different SMART platforms. The occluded part of the stockpile can be easily noticed in these point clouds.

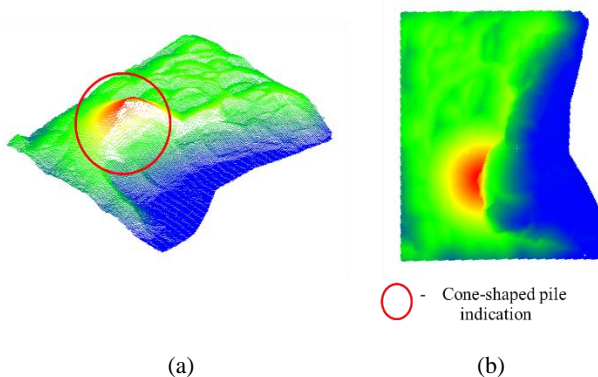


Figure 14. Cone-shaped salt pile captured by Hovermap from (a) perspective and (b) top views.

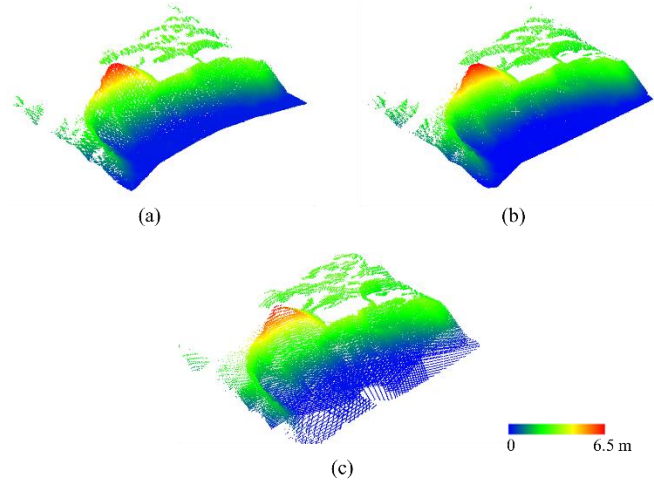


Figure 15. Stockpile area point clouds derived from various SMART systems: (a) SMART Velodyne, (b) SMART Ouster, and (c) SMART Blickfeld.

Figure 16 depicts the impact of the cone-shaped salt pile on the result of interpolation. Areas on the rear side of the cone-shaped salt pile and back-left corner of the stockpile exhibit a large deviation from the reference profile of Hovermap. In both regions, the interpolated point cloud data will lead to an overestimation of the volume. A system that is able to capture such surface variations, even with few points, will produce more accurate results.

Table 5 summarizes the strengths and weaknesses of the three LiDAR units investigated in this study. As introduced earlier, each LiDAR possesses unique characteristics that could be useful in different scenarios of SMART data acquisition and processing. Velodyne VLP16 is a state-of-the-art LiDAR that has a proven reliability. Ouster OS-1-32 is relatively new but provides denser point clouds with a larger vertical FoV. This could be an advantageous feature for mapping large stockpiles with significant surface variations. Moreover, this Ouster unit is rated best among the three for protection against dust and moisture, a common occurrence inside salt storages. In terms of data acquisition and processing, both Velodyne and Ouster benefit from 360-degree horizontal coverage, which enables point cloud registrations with little or no overlap among features. The main downside of these two units is their spinning mechanism, which makes these units less reliable for long term installations and usage inside buildings.

Blickfeld Cube 1 is based on a solid-state technology that eliminates any moving parts. This feature theoretically extends the unit's service life beyond spinning multi-beam LiDAR, which is favorable for permanently installed systems where serviceability is a major concern. With that said, there are challenges associated with using Cube 1. Its limited FoV necessitates smaller rotation increments during data collection to provide sufficient overlap among scans for accurate point cloud registration. This also reduces the versatility of selecting station locations. Thus, from operations and data processing point of view, Velodyne and Ouster SMART are best suited as portable units. On the other hand, Blickfeld Cube 1 is a good candidate for permanent setups inside buildings.

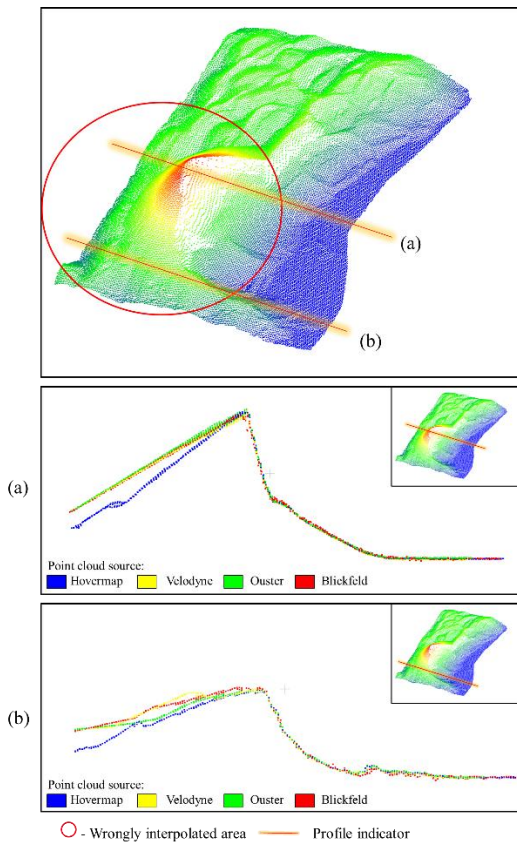


Figure 16. Point clouds profiles showing surface variations after interpolation, (a) profile over the cone-shaped pile (b) profile on the left side of the stockpile.

	Velodyne SMART	Ouster SMART	Blickfeld SMART
LiDAR	-Spinning mechanism -IP67 rated	-Spinning mechanism -IP69K rated	-Solid-state -IP65 rated
LiDAR system calibration	Feature distribution geometry is strong.	Feature distribution geometry is strong.	Feature distribution geometry is weak.
Data processing	Data size is large	Data size is large	Small data size
Volumetric accuracy	Good	Good	Good

Table 5. Technical characteristics of the utilized SMART systems.

6. CONCLUSION

The LiDAR sensors used in this study vary in terms of their operational characteristics (spinning and solid-state), derived point cloud density, and field of view. In the experiment, all three sensor types – Velodyne, Ouster, and Blickfeld produced results with a similar level of volumetric accuracy. The result is most notable for Blickfeld Cube 1, which despite having the least FoV

and highest occlusion achieved a similar level of volumetric accuracy as other SMART units.

Each type of sensor has its own advantages in specific areas. The Velodyne sensor has been consistently reliable, as demonstrated by previous studies. Additionally, it is the most cost-effective option among the sensors that were reviewed. On the other hand, the Ouster sensor generates point clouds with higher density, thanks to its technical features. Lastly, the Blickfeld sensor operates without any spinning components, making it more durable for long-term use. Additional key factor influencing volumetric accuracy of all SMART units is the ability to capture areas that cannot be accurately interpolated during the volume estimation process. Nonetheless, preliminary results from the conducted experiment demonstrate that the three candidate LiDAR units are equally capable to produce volume estimates within a 6% error.

One promising direction for future research lies in testing and evaluating the performance of solid-state LiDAR sensors. The continuous development and rapid emergence of solid-state sensors with improved technical characteristics, such as increased range and wider field of view, offer the potential for more efficient methods of estimating indoor stockpile volumes. Simultaneously, considering scalability factors is crucial, with the initial cost and regular maintenance playing important roles. While the established spinning LiDAR sensors (such as Velodyne VLP16) have a track record of reliability, investing in newer solid-state technology may be worthwhile. These advanced solid-state sensors have the potential to reduce maintenance frequency, leading to long-term cost savings and improved scalability.

ACKNOWLEDGMENT

This work was supported in part by the Joint Transportation Research Program administered by the Indiana Department of Transportation and Purdue University. The contents of this paper reflect the views of the authors, who are responsible for the facts and accuracy of the data presented herein, and do not necessarily reflect the official views or policies of the sponsoring organizations. These contents do not constitute a standard, specification, or regulation.

REFERENCES

- Blickfeld Cube 1 The world’s smallest 3D LiDAR sensor: <https://www.blickfeld.com/lidar-sensor-products/cube-1/> (accessed on April 10th, 2023).
- Desai, J., Mahlberg, J., Kim, W., Sakhare, R., Li, H., McGuffey, J., & Bullock, D. M. (2021). Leveraging telematics for winter operations performance measures and tactical adjustment. *Journal of Transportation Technologies*, 11(4), 611-627.: <https://doi.org/10.4236/jtts.2021.114038>
- Hasheminasab, S. M., Zhou, T., & Habib, A. (2023). Linear Feature-Based Image/LiDAR Integration for a Stockpile Monitoring and Reporting Technology. *IEEE Journal of Selected Topics in Applied Earth Observations and Remote Sensing*, 16, 2605-2623. <https://doi.org/10.1109/JSTARS.2023.3250392>
- He, H., Chen, T., Zeng, H., & Huang, S. (2019). Ground control point-free unmanned aerial vehicle-based photogrammetry for volume estimation of stockpiles carried on barges. *Sensors*, 19(16), 3534. <https://doi.org/10.3390/s19163534>

HOVERMAP(TM). Available online:
<https://www.emesent.io/hovermap/> (accessed on April 10th, 2023).

IP ratings. International Electrotechnical Commission (IEC 60529), Available online: <https://www.iec.ch/ip-ratings> (accessed on July 10th, 2023).

Kelly, V. R., Cunningham, M. A., Curri, N., Findlay, S. E., & Carroll, S. M. (2018). The distribution of road salt in private drinking water wells in a southeastern New York suburban township. *Journal of Environmental Quality*, 47(3), 445-451. <https://doi.org/10.2134/jeq2017.03.0124>

Mahlberg, J. A., Manish, R., Koshan, Y., Joseph, M., Liu, J., Wells, T., & Bullock, D. M. (2022). Salt Stockpile Inventory Management Using LiDAR Volumetric Measurements. *Remote Sensing*, 14(19), 4802. <https://doi.org/10.3390/rs14194802>

Manish, R., Hasheminasab, S. M., Liu, J., Koshan, Y., Mahlberg, J. A., Lin, Y. C., ... & Habib, A. (2022). Image-Aided LiDAR Mapping Platform and Data Processing Strategy for Stockpile Volume Estimation. *Remote Sensing*, 14(1), 231. <https://doi.org/10.3390/rs14010231>

Ouster OS1 Sensor – Mid range:
<https://ouster.com/products/scanning-lidar/os1-sensor/> (accessed on April 10th, 2023).

Raeva, P. L., Filipova, S. L., & Filipov, D. G. (2016). Volume computation of a stockpile—a study case comparing GPS and UAV measurements in an open pit quarry. *The International Archives of the Photogrammetry, Remote Sensing and Spatial Information Sciences*, 41, 999-1004. <http://dx.doi.org/10.5194/isprs-archives-XLI-B1-999-2016>

Ravi, R., Lin, Y. J., Elbahnasawy, M., Shamseldin, T., & Habib, A. (2018). Simultaneous System Calibration of a Multi-LiDAR Multicamera Mobile Mapping Platform. *IEEE Journal of Selected Topics in Applied Earth Observations and Remote Sensing*, 11(5), 1694-1714. <http://dx.doi.org/10.1109/JSTARS.2018.2812796>

Velodyne VLP16 Puck. Available online:
<https://velodynelidar.com/products/puck/> (accessed on April 10th, 2023).

Yilmaz, H. M. (2010). Close range photogrammetry in volume computing. *Experimental Techniques*, 34, 48-54. <https://doi.org/10.1111/j.1747-1567.2009.00476.x>